Dynamic Modeling of a Supersonic Tailless Aircraft with All-moving Wingtip Control Effectors

by

Brady White

Thesis submitted to the faculty of the

Aerospace and Ocean Engineering Department

Virginia Polytechnic Institute and State University

in partial fulfillment of the requirements for the degree of

Master of Science

in

Aerospace Engineering

Dr. William Mason, Committee Chairman

Dr. Chris Hall

Dr. Daniel Inman

Dr. Craig Woolsey

December 7, 2007

Blacksburg, Virginia

Keywords: six degree-of-freedom dynamic model, tailless configuration, all-moving tips

Copyright 2007, Brady White

Abstract

A six degree-of-freedom model for a tailless supersonic aircraft (TSA) concept was developed using MATLAB and Simulink. Aerodynamic data was provided through the computational fluid dynamics analysis of Techsburg, Inc. A three degree-of-freedom model of the configuration's longitudinal dynamics was completed first. Elevator control power was derived from the dynamic response requirements for pitch chosen by Techsburg. The propulsion model utilized General Electric F-414-400-like turbofan engines because an engine deck was readily available. Work on the six degree-of-freedom dynamic model began with determining the necessary rolling and yawing moment coefficients necessary to meet the rest of the chosen dynamic response requirements. These coefficients were then used to find the corresponding all-moving tip deflections. The CFD data showed that even at small all-moving tip deflections the rolling moment coefficient produced was much greater than the amount of yawing moment coefficient produced. This result showed that an additional roll effector was needed to counteract excess rolling moment at any given all-moving tip deflection and trim the aircraft. An angle of attack and pitch rate feedback controller was used to improve the longitudinal dynamics of the aircraft. Because this configuration lacked a vertical tail, a lateral-directional stability augmentation system was vital to its success. The lateral-directional dynamics were improved to Level 1 flying qualities through use of a modified roll/yaw damper. The modified controller fed yaw rate back to both the all-moving tips and roll effector. The six degree-of-freedom model was augmented with

actuator dynamics for the elevator, roll effector, and all-moving tips. The actuators were modeled as first order lags. The all-moving tip actuator time constant was varied to determine the effect of actuator bandwidth on the lateral-directional flying qualities. After the actuator dynamics were successfully implemented, the six degree-of-freedom model was trimmed for both standard cruise and engine-out situations. The eccentuator concept from the DARPA Smart Wing program was selected as a possible conceptual design for the all-moving tip actuation system. The success of the TSA six degree-of-freedom dynamic model proved that morphing all-moving tips were capable of serving as effective control surfaces for a supersonic tailless aircraft.

Acknowledgements

I would like to thank the United States Air Force and Techsburg, Inc. of Blacksburg, Virginia for making this project possible. The project was commissioned and funded by the Air Force. Techsburg was one of the competitors for the second phase of the project. Matt Langford of Techsburg performed all of the computation fluid dynamics for the TSA configuration and supported my dynamic model and stability analysis.

I would like to thank Dr. William Mason for recommending me for this project and acting as the chairman of my graduate committee. I would also like to thank Dr. Daniel Inman and David Neal of the Virginia Tech Center for Intelligent Material Systems and Structures (CIMSS). Dr. Inman provided me with a place to work on my project, and David provided vital guidance that helped me solve any technical problems that arose during the project.

Finally, I would like to thank my parents for supporting me in my academic endeavors. Their support has made my education possible.

Table of Contents

List of Figures

List of Tables

1. Introduction

1.1 Background

The United States Air Force and Navy have been interested in developing new aircraft configurations without vertical stabilizers. Throughout the years, vertical tail size has steadily increased. The elimination of the vertical stabilizer would decrease aircraft weight, drag, and radar cross section while improving speed, range, and payload capability. However, the configuration becomes directionally unstable and lacks directional control (a conventional rudder) when the vertical tail is removed. Alternative control effectors must be developed to provide yaw control to the configuration.

From December 1991 to March 1992, various control effectors were tested in the Wright Patterson Air Force Base Subsonic Aerospace Research Laboratory (SARL) wind tunnel. This wind tunnel is open circuit and low turbulence. It has a contraction ratio of 36 to 1 and a 7x10 ft octagonal cross-section. Each control effector was tested at Mach numbers between 0.3 and 0.5, angles of attack between -5° to 40°, and sideslip angles of -20° to 20°. Vectored thrust was considered as a possible solution for directional control power, but an aerodynamic control surface would be necessary in case of engine failure. Spoilers, clamshell elevons, distributed trailing edge flaps, and all-moving tips were the control effectors tested. The wind tunnel model was a cylindrical fuselage (fineness ratio 6) with a spatular nose (fineness ratio 3). Three different wing planforms using NACA 65-006 airfoils were tested. The planform geometries are summarized in Table 1 and pictured in Figure 1.

Table 1. Geometric parameters for test model wing planforms[1].

Planform	Area (ft^2)	Aspect Ratio	Taper Ratio	LE Sweep (°)	TE Sweep (°)
Delta	2.90	3.2	0.024	50	0
Diamond	2.91	1.53	0.046	50	-50
Parallel	2.86	3.2	N/A	50	50

a) **b)**

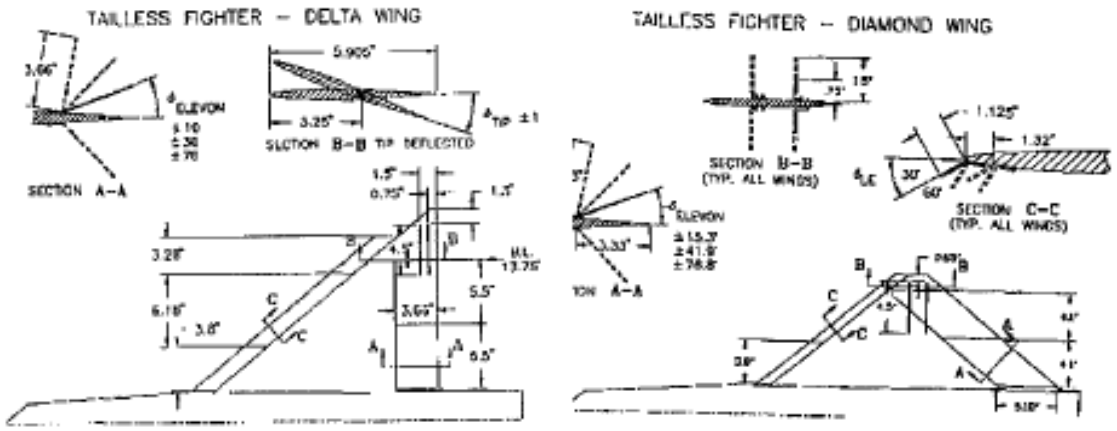

c)

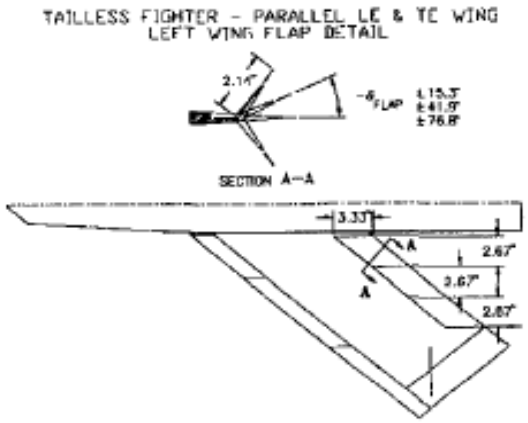

Figure 1. Model wing geometries from SARL wind tunnel test. a) Delta wing planform b) Diamond wing planform c) Parallel leading and trailing edge wing planform[1].

In conventional aircraft designs, spoilers are often used for roll control. They are also capable of causing enough drag to create significant yawing moments. For this wind tunnel test, spoilers were placed on both the top and bottom of the planform and were deflected 90°. The test showed that the spoilers on top of the planform lost effectiveness above 5° angle of attack while the bottom spoilers remained effective over the entire test range. The effect of chordwise spoiler location on yawing moment was found to be very small. When the top and bottom spoilers were deflected simultaneously, the total yawing moment produced was close to the sum of the yawing moment created by each individual spoiler. The amount of yawing moment produced increased with the size of the spoilers. The maximum yawing moment was attained with large spoilers on both the top and bottom of the planform. In this configuration, the spoilers created rolling moment coefficients of less than 0.005 in magnitude at angles of attack up to 10°. The delta planform exhibited very large negative rolling moments above 10° angle of attack while the diamond and parallel planforms showed rolling moments equal to or greater than the yawing moment above 10° angle of attack.

Clamshell elevons were tested on the delta wing and diamond wing planforms at 10°, 30°, and 70° deflections. For the delta wing, the yawing moment was mostly unaffected by changes in angle of attack for the 10° and 30° deflections. Above 10° angle of attack, the 70° deflection showed a large decline in yawing moment production. The rolling moment created was greatly affected by angle of attack changes. The rolling moments were on the order of the yawing moment above 10° angle of attack. The large trailing edge sweep of the diamond wing planform prevents it from producing any significant yawing moment.

All-moving tips were tested on the delta wing and parallel leading and trailing edge wing planforms. These control effectors are useful because they can decouple rolling moment and yawing moment when deflected into a floating position aligned with the local flow angle. To generate roll without yaw, the wingtips are deflected differentially from the floating position producing an equal and opposite load on each tip. Yaw is generated without roll by stalling one of the tips while keeping the other in the floating position. This is similar to the clamshell elevon in that yawing moment is created by differential drag force. However, the tip creates nonlinear rolling moments as it is being stalled. The delta wing planform was tested with streamwise tips. The performance of the all-moving tips deflected +15°/-15° was similar to conventional ailerons. At this deflection, the maximum rolling moment and zero yawing moment were attained at 0° angle of attack. As the angle of attack was increased, the all-moving tips exhibited adverse yaw (yawing motion opposes desired rolling motion) and decreasing rolling moment. Deflections of 0°/-30° and -15°/-45° showed maximum rolling moment at positive angles of attack (6° and 10° respectively). Both deflections showed proverse yaw (yawing motion assists desired rolling motion) and decreases of stability axis yawing moment with increasing angle of attack. The parallel leading and trailing edge wing planform was tested with skewed tips. Rolling moment was nearly constant throughout the test range. The yawing moment was negligible at less than 25° angle of attack. This planform showed small adverse yaw at high angles of attack. The all-moving tip proved to be effective for the delta wing planform, and the parallel wing planform exhibited significant spanwise flow. This suggests that split tip control devices could be effective

for yaw control for delta wing and parallel wing planforms throughout a large flight envelope[1].

Control suites for tailless aircraft were also studied in the Air Force and Navy's Innovative Control Effectors (ICE) program. Phase I of the program began in 1993 and involved identification of aircraft concept, control concepts and power requirements, and integration issues. Baseline concepts were developed for both the Air Force (land-based) and Navy (carrier-based) during this phase. These concepts are shown in Figure 2. The

a) **b)**

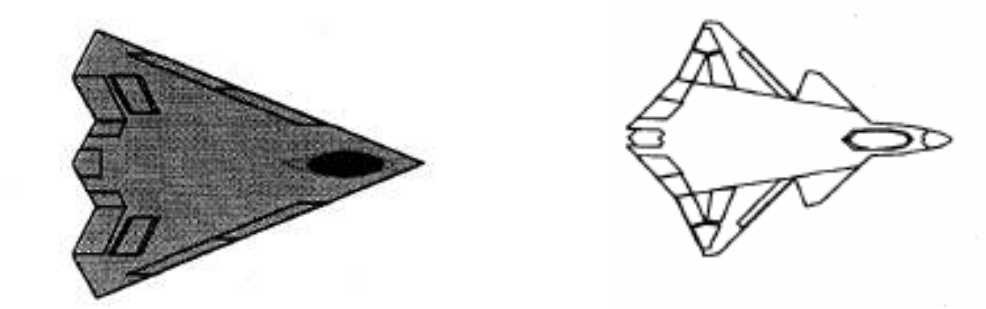

Figure 2. ICE program baseline concepts. a) Air Force land-based concept b) Navy carrier-based concept[2].

Air Force concept was a 65° swept delta wing, and the Navy concept was a diamond wing with a canard. Both concepts had baseline elevons, spoilers, clamshells, leading edge flaps, and thrust vectoring. Innovative effectors added to each concept included all-moving wing tips, differential leading edge flaps, spoiler-slot deflectors, deployable rudder, and lower surface spoilers. Phase II involved wind tunnel tests for the various control effectors. These tests were conducted at the Lockheed Martin Tactical Aircraft Systems Aerodynamic Development Facility, the German LAMP facility, and the Wright Laboratory Subsonic Aerodynamic Research Laboratory.

All-moving tips, spoiler-slot deflectors, and differential leading edge flaps were determined to best satisfy integration, maneuverability, and radar signature requirements. Out of these three control effectors, all-moving tips were evaluated as the best from a performance standpoint. The all-moving tips were much more cost efficient than the baseline configuration due to reduced empty weight, reduced control system complexity, and increased range. When employing all-moving tips, the Air Force concept was 700 lbs lighter than the baseline configuration using spoilers for lateral-directional control. The all-moving tips allowed for increased fuel volume which increased the aircraft range by 16% over the baseline. However, the large actuator fairings for the all-moving tips caused a 4% decrease in transonic acceleration. Multi-axis thrust vectoring was required to meet the Air Force and Navy's high angle of attack roll requirements. Aerodynamic control power alone could not meet these requirements. However, all-moving tips exhibited significant roll performance at high angles of attack without using thrust vectoring[2]. All-moving tips operated with increasing yaw effectiveness at least through deflections of 60°. The effects of sideslip on the yaw effectiveness proved to be negligible. Both straight and skewed all-moving tips were tested in Phase II. The skewed tips provided significantly more control power than the straight tips for a small increase in control surface area[3]. Subsonic wind tunnel tests have validated all-moving tips as a viable roll and yaw effector for tailless aircraft.

1.2 Techsburg, Inc.

The Air Force's Control Effectors for Supersonic Tailless Aircraft (CESTA) program requested proposals from various aerospace companies to develop effective

control suites for tailless aircraft in supersonic flight. Techsburg, Inc. of Blacksburg, Virginia proposed using morphing all-moving tips as control effectors because they have proved to be effective in subsonic flight. However, all-moving tips have not been experimentally validated at supersonic speeds. Morphing tips alleviate some of the aerodynamic and observability penalties of conventional all-moving tips. Both conventional and morphing all-moving tips are shown in Figure 3. Techsburg performed

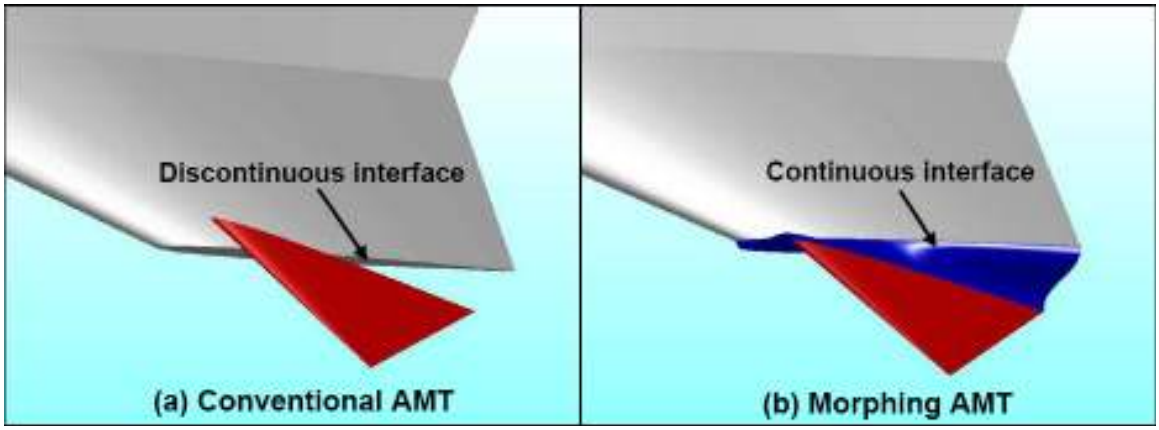

Figure 3. Conventional and morphing all-moving tips deflected at -30°[4] – used with permission of Techsburg, Inc.

aerodynamic analysis of the tailless supersonic aircraft configuration (TSA) using computational fluid dynamics and wind tunnel testing. A similar configuration, the Northrop Grumman Supersonic Tailless Air Vehicle (STAV), is shown in Figure 4. The author was supported by Techsburg to build the dynamic model and control system for the configuration from the aerodynamic data. This thesis describes the development of the TSA six degree-of-freedom dynamic model and control system using all-moving tips.

Figure 4. Northrop Grumman Supersonic Tailless Air Vehicle (STAV) configuration[5].

2. Dynamic Model Development

2.1 TSA Configuration

Techsburg chose the TSA as the baseline configuration for computational fluid dynamics (CFD) analysis. The TSA was designed to cruise at Mach 1.6 at 35,000 ft with Level 1 flying qualities. Techsburg performed all CFD analysis at Mach 1.6 and 35,000 ft using GASP, a well-known CFD flow solver that solves the Reynolds Averaged Navier-Stokes equations. The 1-equation Spalart-Allmaras Tu model was used as the turbulence model[6]. For zero sideslip cases, 1.94 million cells were used with the configuration centerline as a symmetry plane. 3.9 million cells were used for cases involving sideslip. Negative elevator and AMT deflections implied upward deflections of the control surfaces, and positive deflections implied downward control surface deflections. From the CFD results, the static margin of the TSA at these flight conditions was determined to be 0.138. Despite lacking a conventional horizontal stabilizer, the TSA was longitudinally stable at these conditions due to the supersonic c.g. shift. The TSA longitudinal aerodynamic coefficients are shown in Figure 5. Necessary control power for the TSA was determined from high speed dynamic response requirements chosen by Techsburg. These requirements are shown in Table 2.

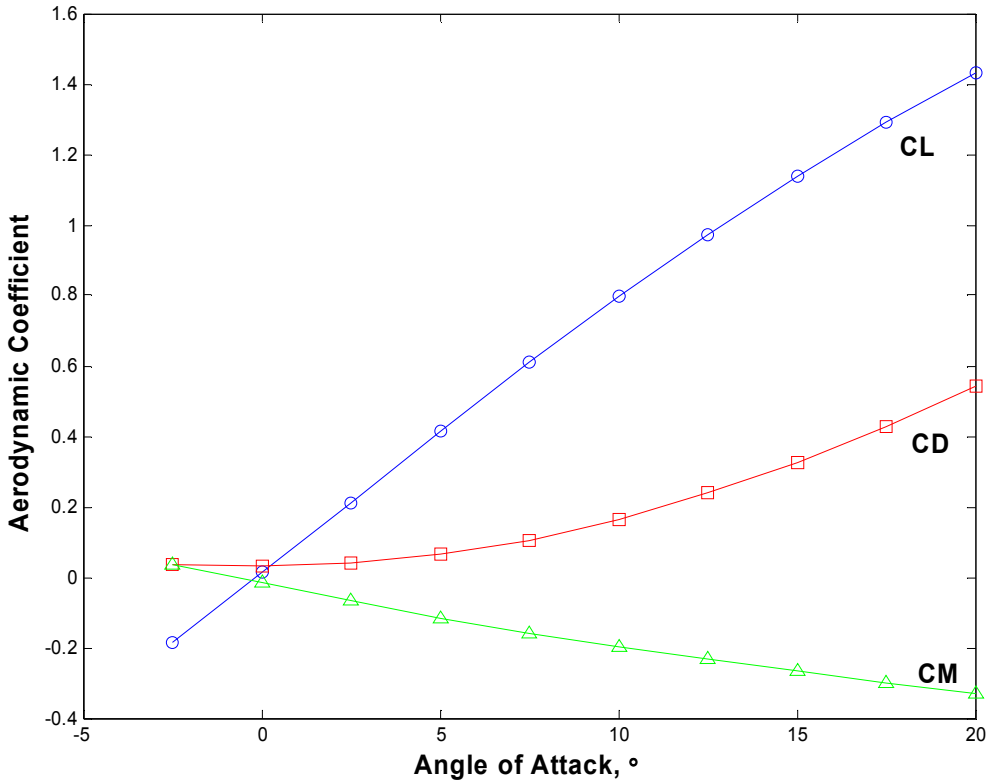

Figure 5. Lift coefficient, drag coefficient, and pitching moment coefficient variation with angle of attack (M = 1.6, h = 35,000 ft).

Table 2. TSA supersonic dynamic response requirements.

Roll Requirements		**Pitch Requirements**		**Yaw Requirements**	
Steady-state Roll Rate	50°/sec	**Steady-state Pitch Rate**	50°/sec	**Sideslip Angle**	5°
Roll Acceleration	100°/sec^2	**Pitch Acceleration**	50°/sec^2	**Yaw Acceleration**	10°/sec^2

2.2 Propulsion Model

The TSA is a two engine configuration. Because no other propulsion data was given, assumptions were made to create the propulsion model. An engine deck for a F-414-400-like engine was available from an AIAA undergraduate design competition. Because this engine data was readily available, it was used as the powerplant in the

aircraft propulsion model. While two of these engines suffice for the Navy's F-18E/F, four are required to propel the aircraft in trimmed flight at Mach 1.6. For the dynamic model, only two F-414-400-likes were used, but their thrust output was doubled. The angular momentum produced by each engine was assumed to be 160 slug-ft^2/sec (from an F-16 engine model)[7]. The engine deck gave thrust as a function of fifteen power settings with settings of eleven and above being afterburning. These power settings were converted into throttle settings with PS 15 corresponding to full throttle. A quadratic curve was fit then through the data. The effects of throttle setting on output thrust for both two and four F-414-400-likes are shown in Figure 6. The four engines are equivalent to the two double powered engines used in the model.

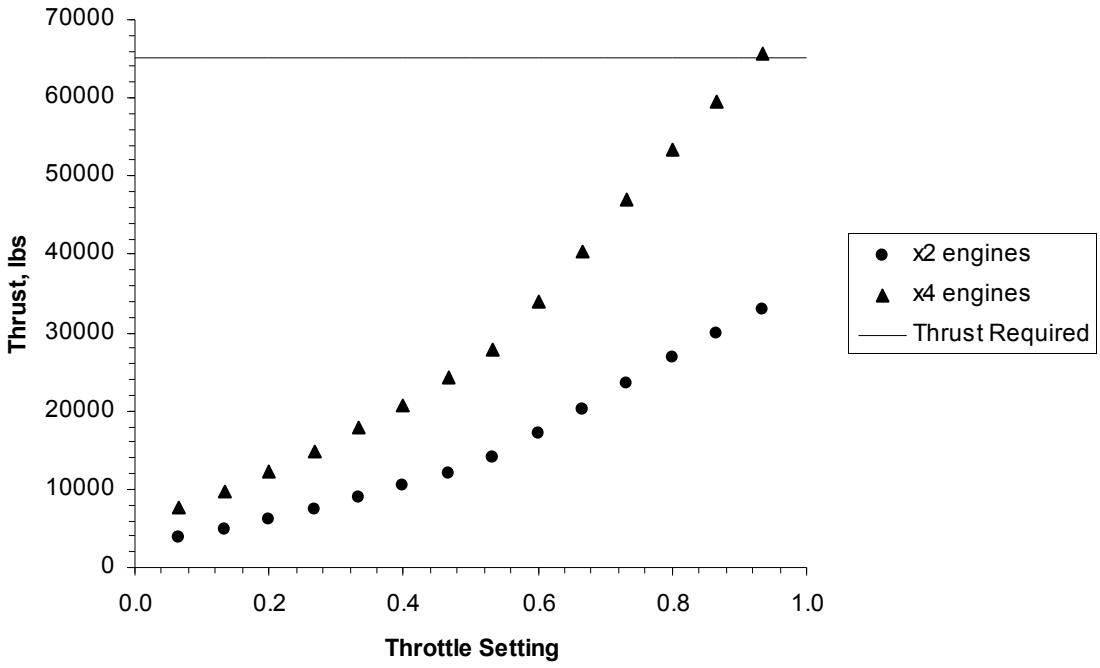

Figure 6. Thrust generated by F-414-400-like engines.

2.3 TSA 3 Degree-of-Freedom Dynamic Model

A simple 3 degree-of-freedom model of the TSA longitudinal dynamics was created first. The F-16 dynamic model from Stevens and Lewis was used as a basis for the TSA model. The model was implemented in MATLAB using Simulink and s-functions. Once the TSA parameters were used in the model, the TRIM Simplex algorithm from Stevens and Lewis was used to find a trim throttle setting and elevator deflection. This algorithm was converted from FORTRAN to MATLAB by David Neal.

An estimate of the elevator control power was needed for the dynamic model. Elevator control power is found in the equation for the total aircraft pitching moment

$$C_{MTotal} = C_{MBase} + C_{M\delta e}\delta e \quad \textbf{(1)}$$

where C_{MBase} is the pitching moment from the CFD and $C_{M\delta e}$ is the change in pitching moment with elevator deflection. To determine $C_{M\delta e}$, the equations for a Stevens and Lewis-defined pitch damping term (Eq. 2) and pitch acceleration (Eq. 3) were solved for total pitching moment (Eq. 4).

$$D_{pitch} = \frac{\bar{c}(C_{MQ}Q + C_{M\dot{\alpha}}\dot{\alpha})}{V_T} \quad \textbf{(2)}$$

$$\dot{Q} = \frac{\bar{q}S\bar{c}(C_M + D_{pitch}) + Tz_E}{I_{yy}} \quad \textbf{(3)}$$

$$C_M = \frac{\dot{Q}I_{yy} - Tz_E}{\bar{q}S\bar{c}} - D_{pitch} \quad \textbf{(4)}$$

The dynamic requirements were input as the pitch rate and pitch acceleration. The pitch damping stability derivative (C_{MQ}) was obtained from CFD data, and $C_{M\dot{\alpha}}$ was assumed to be negligible[7]. Once the total pitching moment was found, it was entered into

Equation 1 to find $C_{M\delta e}$. Using an arbitrarily chosen 2° angle of attack and -5° elevator deflection, $C_{M\delta e}$ was calculated to be -0.01051 /°. Thus, this was assumed to be the minimum elevator control power necessary for basic maneuvering. The trim conditions for the longitudinal dynamic model are shown in Table 3.

Table 3. Three degree-of-freedom dynamic model trim conditions.

Mach Number	1.6
Altitude (ft)	35,000
Throttle Setting	0.9037
Angle of Attack (°)	0.426
Elevator Deflection (°)	-2.35

2.4 TSA 6 Degree-of-Freedom Dynamic Model

The full dynamic model (Appendix 7.3) was started upon completion of the longitudinal model. As in the previous model, the effectiveness of the lateral-direction control surfaces needed to be identified. The forces and moments generated by the all-moving tips (AMT) were determined from CFD analysis and plotted against AMT deflection. This plot is shown in Figure 7. These data were curve fit and used in the model as the various lateral-directional control power derivatives. The rolling moment coefficient was linear with AMT deflection while both the yawing moment coefficient and side force coefficient exhibited quadratic relationships. The relationship between rolling moment coefficient and yawing moment coefficient was favorable (rolling moment and yawing moment decrease together) for negative AMT deflections and adverse (rolling moment decreases with increasing yawing moment) for positive AMT deflections.

The maximum AMT deflection needed to meet the dynamic response requirements from Table 2 was required so that Techsburg could begin manufacturing models for wind tunnel testing. Various assumptions were needed to complete this analysis. As mentioned previously, the angular momentum of each engine (H_E) was assumed to be 160 sl-ft^2/sec. Because the TSA is a flying wing configuration, the cross-product of inertia I_{xz} was assumed to be negligible[8]. Most of the dynamic damping derivatives (C_{LR}, C_{LP}, C_{NR}, and C_{NP}) were taken from the CFD analysis. However, both C_{YR} and C_{YP} were assumed to be negligible[9]. The total required rolling and yawing moment coefficients were derived from the equations of motion for roll rate and yaw rate

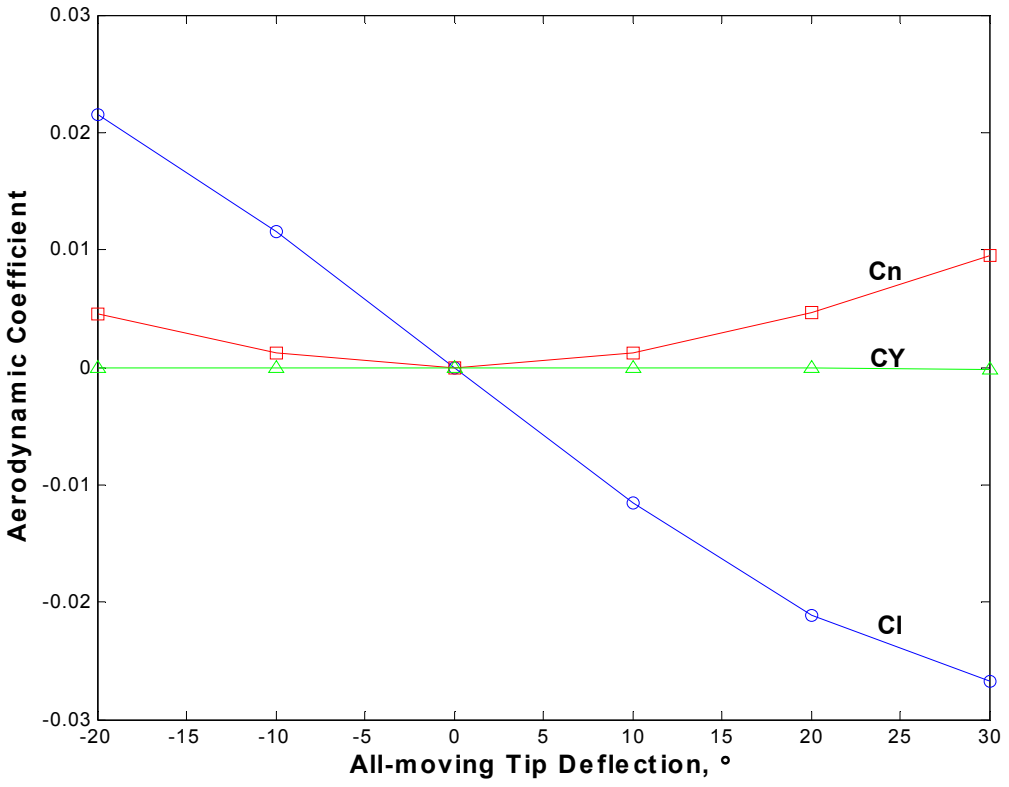

Figure 7. Rolling moment coefficient, yawing moment coefficient, and side force coefficient variation with AMT deflection (M = 1.6, h = 35,000 ft) – only right tip is deflected.

$$\dot{P} = Q(C_2 P + C_1 R + C_4 H_E) + \bar{q} Sb(C_3 C_{LTotal} + C_4 C_{NTotal}) \quad \textbf{(5)}$$

$$\dot{R} = Q(C_8 P - C_2 R + C_9 H_E) + \bar{q} Sb(C_4 C_{LTotal} + C_9 C_{NTotal}) \quad \textbf{(6)}$$

where an arbitrary yaw rate of 25°/sec was added to the analysis. Eqs. (5) and (6) were solved for rolling moment coefficient and yawing moment coefficient yielding

$$C_L = \frac{A_1 - \frac{C_4}{D}(C_3 A_2 - C_4 A_1)}{C_3} \quad \textbf{(7)}$$

$$C_N = \frac{C_3 A_2 - C_4 A_1}{D} \quad \textbf{(8)}$$

where the coefficients A_1, A_2, and D are equal to

$$A_1 = \frac{\dot{P} - (C_2 P + C_1 R + C_4 H_E) Q}{\bar{q} Sb} \quad \textbf{(9)}$$

$$A_2 = \frac{\dot{R} - (C_8 P - C_2 R + C_9 H_E) Q}{\bar{q} Sb} \quad \textbf{(10)}$$

$$D = C_3 C_9 - C_4^2 \quad \textbf{(11)}$$

The total rolling and yawing moment coefficients required to meet the dynamic response requirements (50°/sec steady-state roll rate, 100°/sec^2 roll acceleration, 5° sideslip angle, and 10°/sec^2 yaw acceleration) were determined to be 0.002291 and 0.002109 respectively. In the equations of motion, these coefficients are equal to

$$C_{LTotal} = C_{LBase} + C_{Lc.d.} + \frac{b}{2V_T}(C_{LR} R + C_{LP} P) \quad \textbf{(12)}$$

$$C_{NTotal} = C_{NBase} + C_{Nc.d.} + \frac{b}{2V_T}(C_{NR} R + C_{NP} P) - C_{YTotal} \frac{(x_{cgr} - x_{cg})}{b} \quad \textbf{(13)}$$

where the total side force coefficient C_{Ytotal} is

$$C_{YTotal} = C_{YBase} + C_{Yc.d.} + \frac{b}{2V_T}(C_{YR} R + C_{YP} P) \quad \textbf{(14)}$$

The *c.d.* subscript refers to the coefficient due to control deflection[7]. These terms are equal to the curve fits obtained previously. Thus, the c.d. terms are governed by AMT deflection. The *base* subscript terms are equivalent to the force and moment coefficients from the CFD analysis. The necessary control deflections to meet the dynamic response requirements were calculated by iterating AMT deflections in MATLAB until numerical solutions were found to Eqs. (12) and (13). This analysis was performed at both -5° sideslip and the required 5° sideslip. These results are found in Table 4. The AMT deflections at positive 5° sideslip clearly show a large difference between the

Table 4. AMT deflections necessary to meet dynamic response requirements.

	AMT deflection to meet C_{LTotal}	**AMT deflection to meet C_{NTotal}**
-5° sideslip	-7.786°	-8.149°
+5° sideslip	-2.726°	-17.564°

deflection to obtain the required rolling moment coefficient and the deflection to obtain the required yawing moment coefficient. The results also were used to determine the necessary maximum AMT deflection of 20°. Techsburg machined a series of test models up to the maximum AMT deflection for use in wind tunnel testing. These wind tunnel tests were used to validate the aerodynamic data from CFD.

Figure 7 shows that the rolling moment coefficient is at least an order of magnitude higher than the yawing moment coefficient at a given AMT deflection. An AMT deflection to meet a yawing requirement will generate excess rolling moment that will prevent the aircraft from trimming. Thus, an additional roll effector is needed to rid the configuration of excess rolling moment and trim the aircraft. The roll effector was modeled by adding an extra term to the total rolling moment coefficient expression to get

$$C_{LTotal} = C_{LBase} + C_{Lc.d.} + \frac{b}{2V_T}(C_{LR}R + C_{LP}P) + REFF \qquad \textbf{(15)}$$

where REFF is the rolling moment coefficient generated by the new roll effector. An elevon or other similar control effector would be a likely candidate for the roll effector. The addition of the lateral-directional dynamics slightly altered the model trim conditions due to limited numerical precision. This imprecision resulted in a very small, but nonzero, pitching moment. Because the lateral-directional dynamics are unstable, the nonzero pitching moment creates both roll and yaw which is then driven back to zero by the lateral-directional control system. The effects of these additional moments and the controller result in new longitudinal trim conditions. The trim conditions for the six degree-of-freedom dynamic model are shown in Table 5.

Table 5. Six degree-of-freedom dynamic model trim conditions.

Mach Number	1.6
Altitude (ft)	35,000
Throttle Setting	0.8926
Angle of Attack (°)	0.6244
Elevator Deflection (°)	-1.7220

2.5 Actuator Dynamics

Actuator dynamics for elevator, all-moving tip, and roll effector actuators were added to the six degree-of-freedom dynamic model. The linearized aircraft dynamics were modeled in the typical state space form

$$\dot{x} = Ax + Bu \tag{16}$$

with state matrix A and control matrix B. As suggested by Stevens and Lewis, each actuator was modeled as a first order lag[7]

$$\dot{x}_a = \frac{u - x}{\tau} \tag{17}$$

where the time constant τ was assumed to be 0.05 sec (3.183 Hz) for each actuator[10]. Eqs. (16) and (17) were combined to put the aircraft and actuator dynamics in the state space form

$$\frac{d}{dt}\begin{bmatrix} x_s \\ x_a \end{bmatrix} = \begin{bmatrix} A & B \\ 0 & -\frac{1}{\tau} \end{bmatrix}\begin{bmatrix} x_s \\ x_a \end{bmatrix} + \begin{bmatrix} 0 \\ \frac{1}{\tau} \end{bmatrix} U_{com} \tag{18}$$

where the commanded power U_{com} is

$$U_{com} = \begin{bmatrix} K_s & K_a \end{bmatrix}\begin{bmatrix} x_s \\ x_a \end{bmatrix} \tag{19}$$

with control gains for both the aircraft state (K_s) and actuators (K_a). Next, Eqs. (18) and (19) were combined to find the final state space form

$$\frac{d}{dt}\begin{bmatrix} x_s \\ x_a \end{bmatrix} = \begin{bmatrix} A & B \\ \frac{K_s}{\tau} & -\frac{1}{\tau} + \frac{K_a}{\tau} \end{bmatrix}\begin{bmatrix} x_s \\ x_a \end{bmatrix} + \begin{bmatrix} 0 \\ \frac{1}{\tau} \end{bmatrix} U_{com} \tag{20}$$

The AMT actuator time constant was varied to determine its effects on the TSA lateral-directional flying qualities. This study will be discussed later in the lateral-directional control system section of the next chapter.

3. Control Systems Development

3.1 Longitudinal Stability Augmentation System

The TSA configuration was longitudinally stable at Mach 1.6 with a static margin of 0.138. Although a control system was not required to stabilize the longitudinal dynamics, a controller was used to improve the longitudinal flying qualities. A pitch rate and alpha feedback controller was used as the longitudinal stability augmentation system. A diagram of this controller is shown in Figure 8. This type of controller uses separate gains for the angle of attack and pitch rate to control elevator deflection.

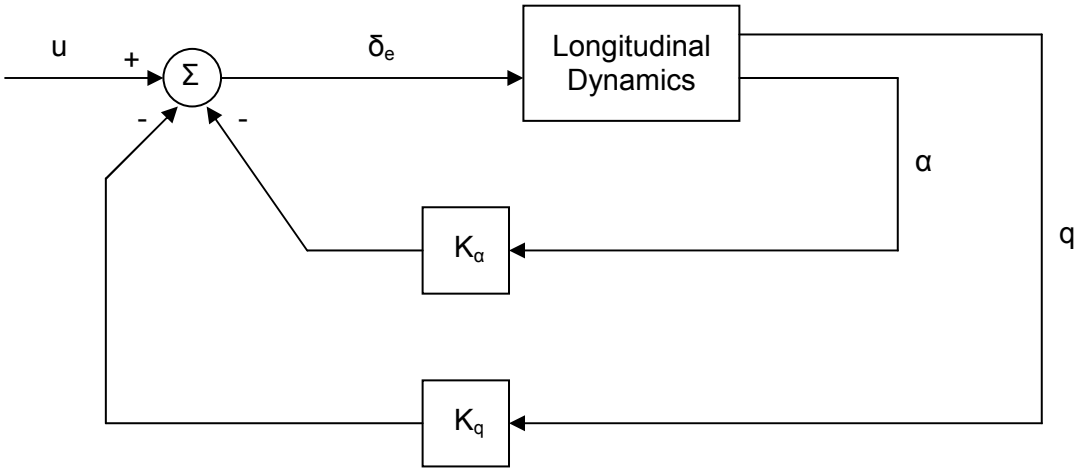

Figure 8. TSA longitudinal stability augmentation system.

The controller design began with the open loop representation of the aircraft dynamics linearized about trim conditions. The open loop poles were located at -1.37 ± 10.33i (short period mode), -0.010 ± 0.027i (phugoid mode), and -20 (elevator actuator). The angle of attack control gain (K_α) was found using the root locus diagram

of the angle of attack to elevator deflection transfer function. The root locus diagram is shown in Figure 9. This first loop closure was used to increase the damping ratio for the short period mode.

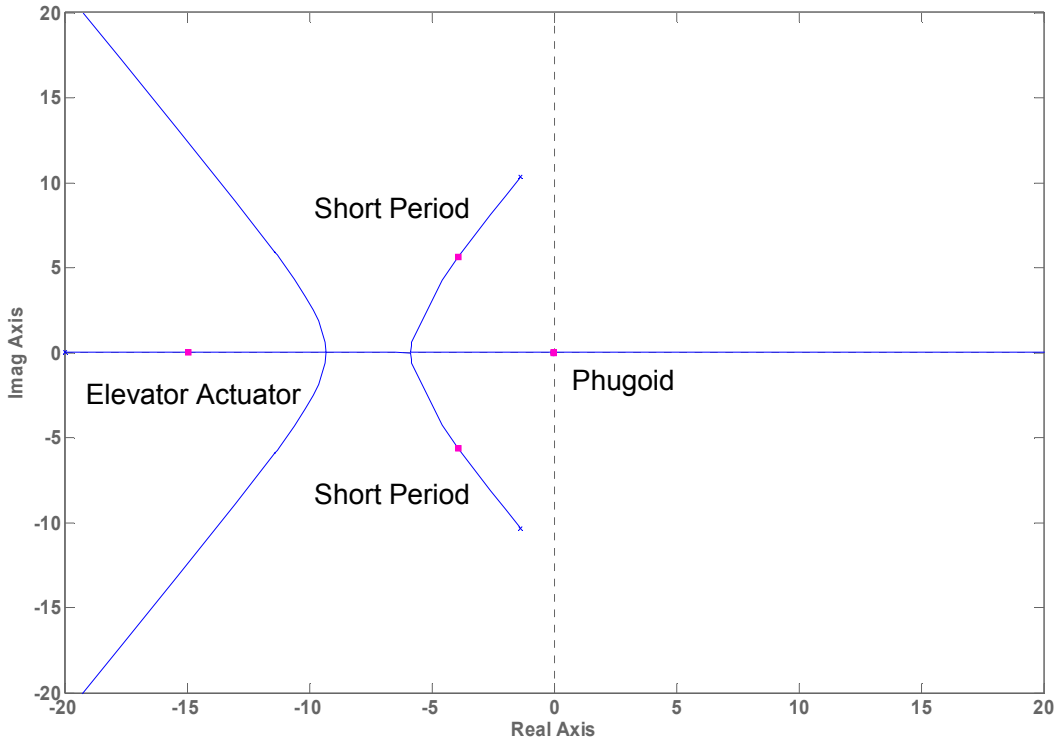

Figure 9. Root locus diagram for angle of attack to elevator deflection transfer function ($K_\alpha = 39.6$).

A second loop closure was used to slightly adjust the short period mode damping and natural frequency. The pitch rate control gain (K_q) was determined from root locus analysis of the transfer function of pitch rate to elevator deflection. The root locus diagram is shown in Figure 10. The longitudinal stability augmentation system was implemented with the control gains $K_\alpha = 39.6$ and $K_q = 0.000254$. The final closed loop poles for the longitudinal dynamics were -4.45 ± 4.53i (short period mode), -0.010 ± 0.026i (phugoid mode), and -13.9 (elevator actuator). The resulting longitudinal flying

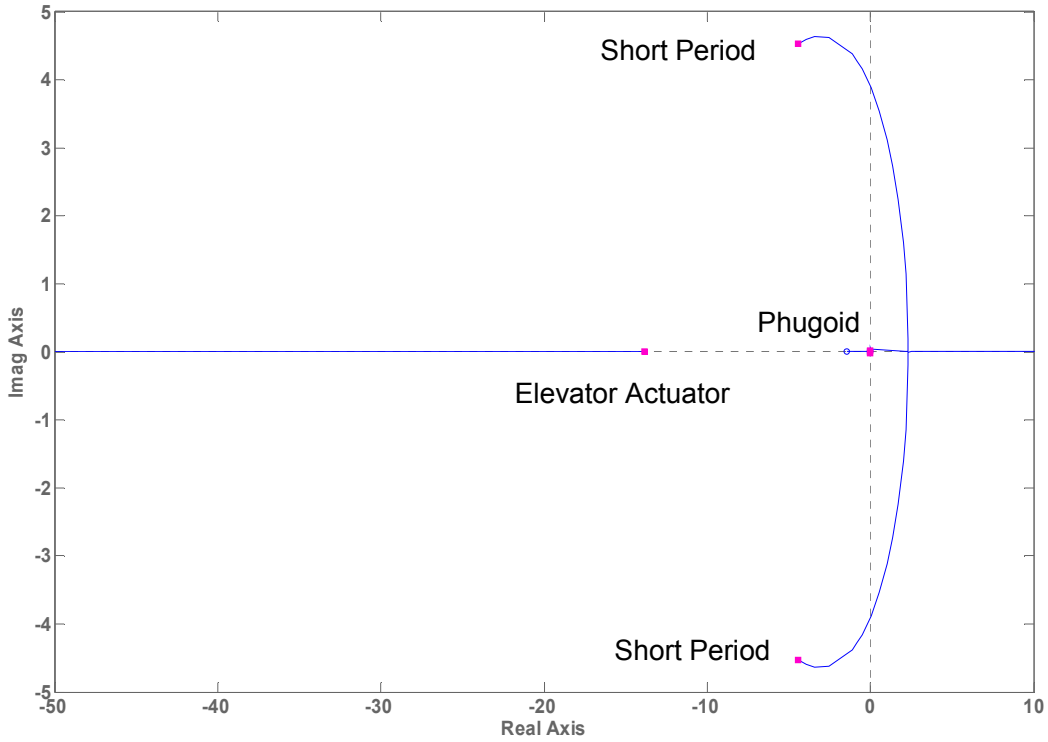

Figure 10. Root locus diagram for pitch rate to elevator deflection transfer function (K_q = 0.000254).

qualities both with and without the controller are summarized in Table 6. The controller mainly improved the short period mode characteristics. The TSA was stable and met all Level 1 flying qualities with and without the stability augmentation system. Longitudinal Level 1 flying qualities will be discussed in more detail in the following chapter.

Table 6. TSA longitudinal open and closed loop performance.

		Without SAS	With SAS
Phugoid mode	Damping Ratio	0.3450	0.3540
	Natural Frequency	0.02898	0.02823
Short Period mode	Damping Ratio	0.1316	0.7002
	Natural Frequency	10.2416	6.3485
	$\omega_n^2/(n/\alpha)$	1.1837	0.4392
Elevator actuator	Pole Location	-20	-13.9

3.2 Lateral-Directional Stability Augmentation System

A lateral-directional stability augmentation system was imperative to the success of the TSA. Because this configuration lacked a vertical tail, it was inherently directionally unstable. The lateral-directional controller was initially implemented using simple pole placement techniques. This controller was adequate until actuator dynamics were added to the model. Using the pole placement controller, the aircraft could not be stabilized with actuator dynamics. Next, a roll/yaw damper stability augmentation system was attempted. This controller also failed to successfully stabilize the lateral-directional dynamics. Finally, a heavily modified roll/yaw damper approach was successful. Instead of feeding back roll rate to the main roll effector (the added roll effector) and yaw rate to the main yaw effector (AMT), this new approach fed yaw rate to both lateral-directional control effectors. The roll rate feedback had negligible effect on the Dutch roll mode flying qualities due to pole-zero cancellations. This controller is shown in Figure 11.

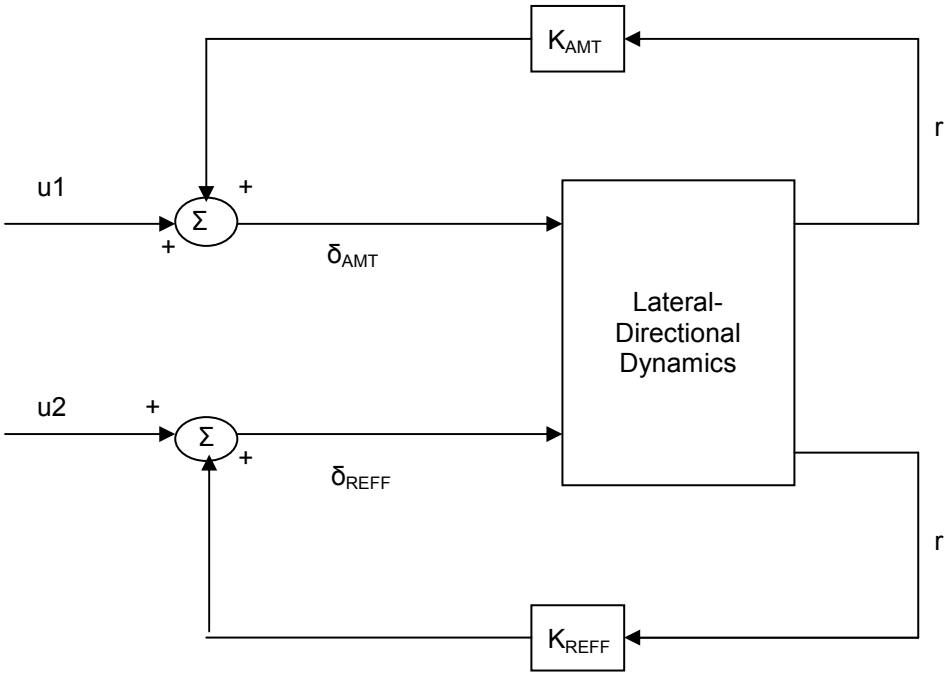

Figure 11. TSA lateral-directional stability augmentation system.

As with the longitudinal controller, the lateral-directional open loop poles were found for the linearized aircraft dynamics. The open loop poles were located at 0.0068 ± 18.9i (Dutch roll mode), 0.0008 (spiral mode), -3.76 (roll subsidence mode), and -20 (AMT and roll effector actuators). Both the Dutch roll and spiral modes were unstable in the open loop. The roll effector control gain (K_{REFF}) was found using the root locus diagram of yaw rate to roll effector deflection transfer function. Using negative control gains, the unstable Dutch roll mode became more unstable with increasing gain magnitude. However, the Dutch roll poles were pulled into the left half-plane of the root locus using positive control gains. The root locus diagram is shown in Figure 12. This first loop closure was used to stabilize the Dutch roll mode and place the Dutch roll poles so that they met Level 1 flying qualities for damping ratio. This approach caused the spiral mode to become more unstable. Although Level 1 flying qualities allow for a

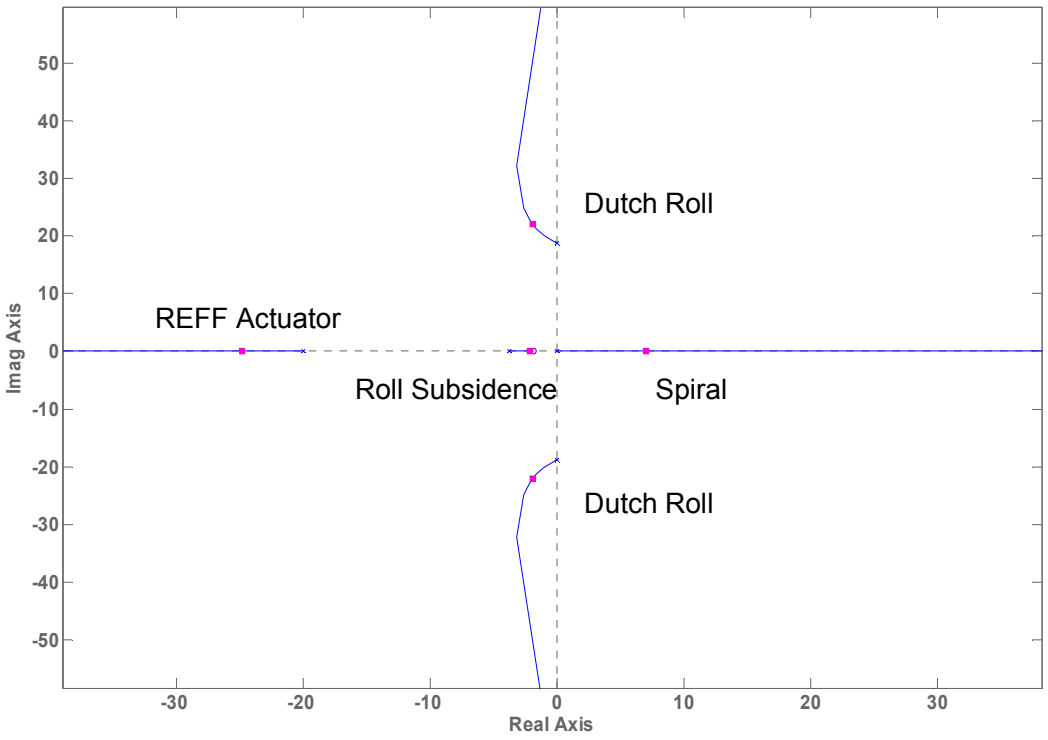

Figure 12. Root locus diagram for yaw rate to roll effector deflection transfer function (K_{REFF} = 0.254).

limited amount of instability in the spiral mode, a second loop closure was used to stabilize it. Both the roll subsidence mode and all-moving tip actuator remained stable.

A second loop closure using the yaw rate to all-moving tip deflection transfer function was used to stabilize the spiral mode. The all-moving tip control gain (K_{AMT}) was determined from a root locus analysis of this transfer function. As before, a positive control gain was necessary for stabilization. This root locus diagram is shown in Figure 13. With this second loop closure, all lateral-directional modes were made stable and had their flying qualities improved.

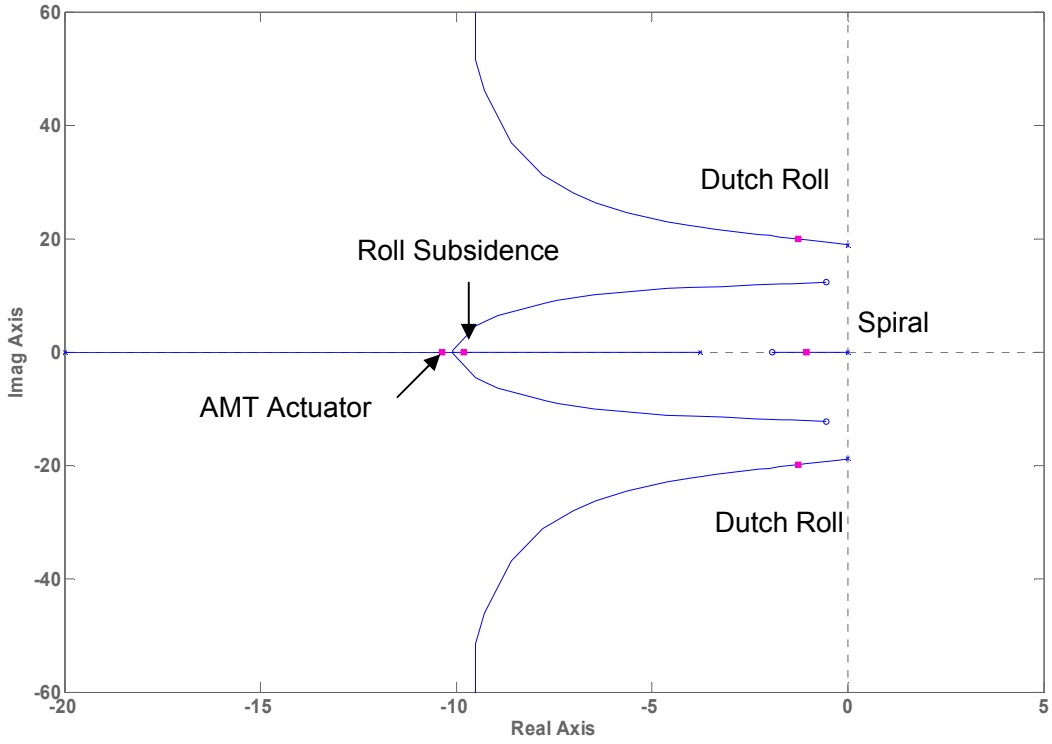

Figure 13. Root locus diagram for yaw rate to all-moving tip deflection transfer function (K_{AMT} = 323).

This controller was implemented with the control gains K_{AMT} = 323 and K_{REFF} = 0.248. The final closed loop poles were located at -1.78 ± 20.6i (Dutch roll mode), -1.06 (spiral mode), -9.92 (roll subsidence mode), -24.6 (roll effector actuator), and -10.2 (AMT actuator). The resulting dynamics with and without the controller are summarized in Table 7. The lateral-directional stability augmentation system effectively stabilized the Dutch roll and spiral modes and improved the roll subsidence mode performance. With the lateral-directional controller, the TSA was made flyable and met all Level 1 flying qualities. Lateral-directional Level 1 flying qualities will be discussed in more detail in the next chapter.

Table 7. TSA lateral-directional open and closed loop performance.

		Without SAS	With SAS
Dutch Roll mode	Damping Ratio	-0.0004	0.086
	Natural Frequency	18.8559	20.7
Roll Subsidence mode	Time constant	0.26618 sec	0.10081 sec
Spiral mode	Time to double amplitude	842.2 s	stable (exponential decay)
AMT actuator	Pole Location	-20	-24.6
Roll Effector actuator	Pole Location	-20	-10.2

3.3 Actuation Systems Concept

Concepts for the all-moving tip actuation system were also explored. Techsburg's CFD analysis showed that 22,127 ft-lb of torque were required to deflect an AMT 20° at Mach 1.6. A search for a viable and commercially available actuation system proved unsuccessful. However, newer technologies may offer solutions for the morphing AMT actuation system design. A possible candidate is the eccentuator concept used in the DARPA Smart Wing program. The eccentuator, shown in Figure 14, is essentially a deformable beam capable of converting input torques on one end into vertical forces on the other end. An example conceptual design exhibiting the morphing capabilities of eccentuators is shown in Figure 15. Unfortunately, the exact torque and bandwidth capabilities of the eccentuator concept are not readily available at this time. Present eccentuator technology may be insufficient for the high control hinge moments

experienced at supersonic speeds[11]. Further work is needed to determine a capable actuator for the TSA morphing AMT system.

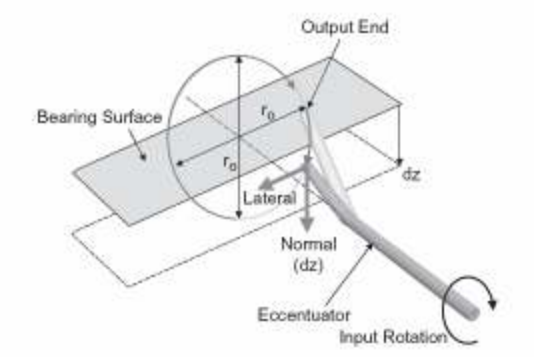

Figure 14. Eccentuator concept schematic[11] – used with permission of Sage Publications.

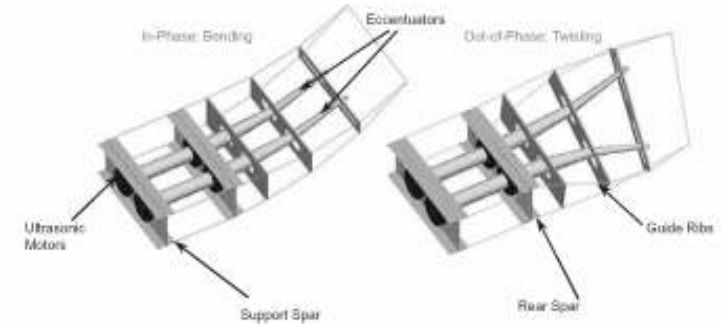

Figure 15. Conceptual morphing wing actuation system design with eccentuators[11] – used with permission of Sage Publications.

4. Control Systems Performance

4.1 Level 1 Flying Qualities Requirements

The desired flying qualities of the TSA configuration were chosen so that both longitudinal and lateral-directional Level 1 flying qualities were met for each dynamic mode. At the Mach 1.6 test condition, the longitudinal dynamic modes were stable and met Level 1 flying qualities without a stability augmentation system. However, a control system was implemented to improve the existing longitudinal dynamics. Table 8 shows the longitudinal flying qualities with and without the controller and how they compare to the Level 1 requirements.

Table 8. TSA longitudinal Level 1 flying qualities.

		Level 1 requirement	**Without SAS**	**With SAS**
Phugoid mode	Damping Ratio	$\zeta \geq 0.04$	0.3450	0.3540
	Natural Frequency		0.02898	0.02823
Short Period mode	Damping Ratio	$0.30 \leq \zeta \leq 2.00$	0.1316	0.7002
	Natural Frequency	$\omega_n \geq 1.0$	10.2416	6.3485
	$\omega_n^2/(n/\alpha)$	$0.085 \leq \omega_n^2/(n/\alpha) \leq 3.60$	1.1837	0.4392

Due to the tailless nature of the configuration, many of the lateral-directional dynamic modes were unstable at Mach 1.6. A lateral-directional stability augmentation system was necessary to stabilize the dynamics and meet Level 1 flying qualities. Table 9 shows the lateral-directional flying qualities with and without the controller and how they compare to the Level 1 requirements. The control systems successfully stabilized the TSA dynamics and allowed it to meet all required Level 1 flying qualities.

Table 9. TSA lateral-directional flying qualities.

		Level 1 requirement	Without SAS	With SAS
Dutch Roll mode	Damping Ratio	$\zeta \geq 0.08$	-0.0004	0.086
	Natural Frequency	$\omega_n \geq 0.4$	18.8559	20.7
		$\zeta\, \omega_n \geq 0.15$	-0.0075	1.7802
Roll Subsidence mode	Time constant	$\tau \leq 1.4$ sec	0.26618 sec	0.10081 sec
Spiral mode	Time to double amplitude	$T_2 \geq 20$ s	842.2 s	stable (exponential decay)

4.2 Controller Response to Perturbations and Engine-out

Both the longitudinal and lateral-directional control systems were designed using the linearized aircraft dynamics. To make sure that the controller could handle perturbations to the trim conditions, small disturbances were added to the full six degree-of-freedom model as initial conditions. Figure 16 shows the system response to an initial 2° angle of attack, and Figure 17 shows the response to an initial 3° sideslip. In each case, the TSA model was successfully returned to the trim conditions.

The controller was also tested for engine-out situations. Engine-out conditions were simulated by adding the moment from a single engine to the yawing moment coefficient. Longitudinal trim was maintained by keeping the thrust and elevator inputs at their trim values. Maintaining the longitudinal trim in engine-out was unrealistic, but the purpose of the study was to test the lateral-directional control system in an engine-out situation. The control system kept the TSA trimmed throughout the engine-out simulation. The engine-out trim conditions are shown in Table 10. Figure 18 shows the AMT and roll effector deflections during the engine-out simulation.

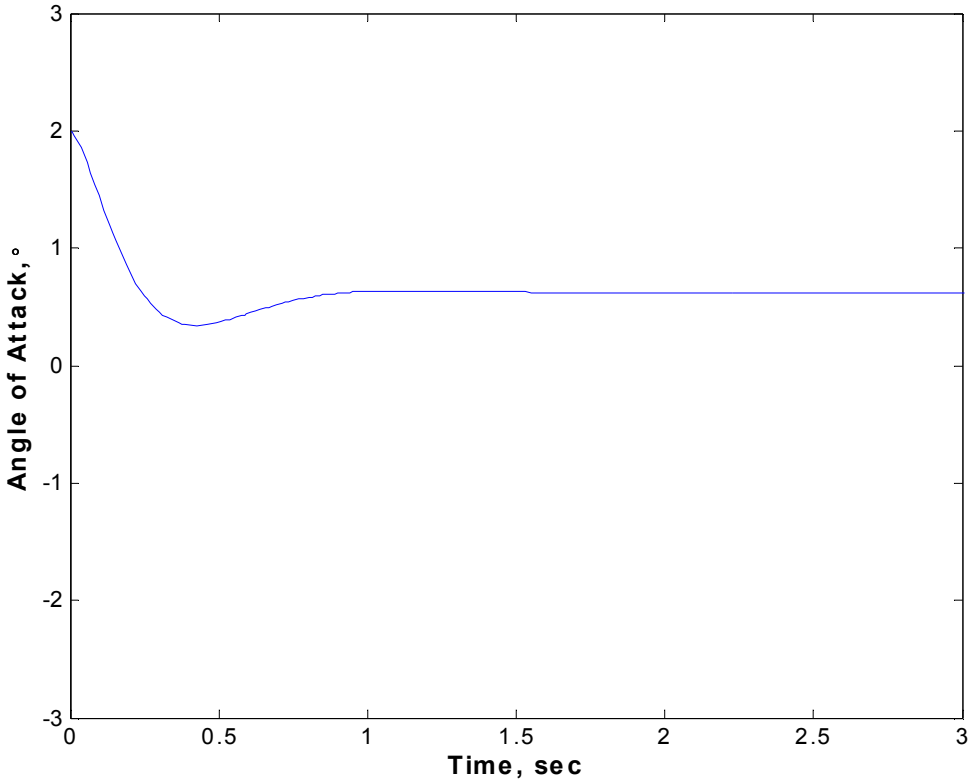

Figure 16. TSA response to initial 2° angle of attack (α_{trim} = 0.6244°, M = 1.6, h = 35,000 ft).

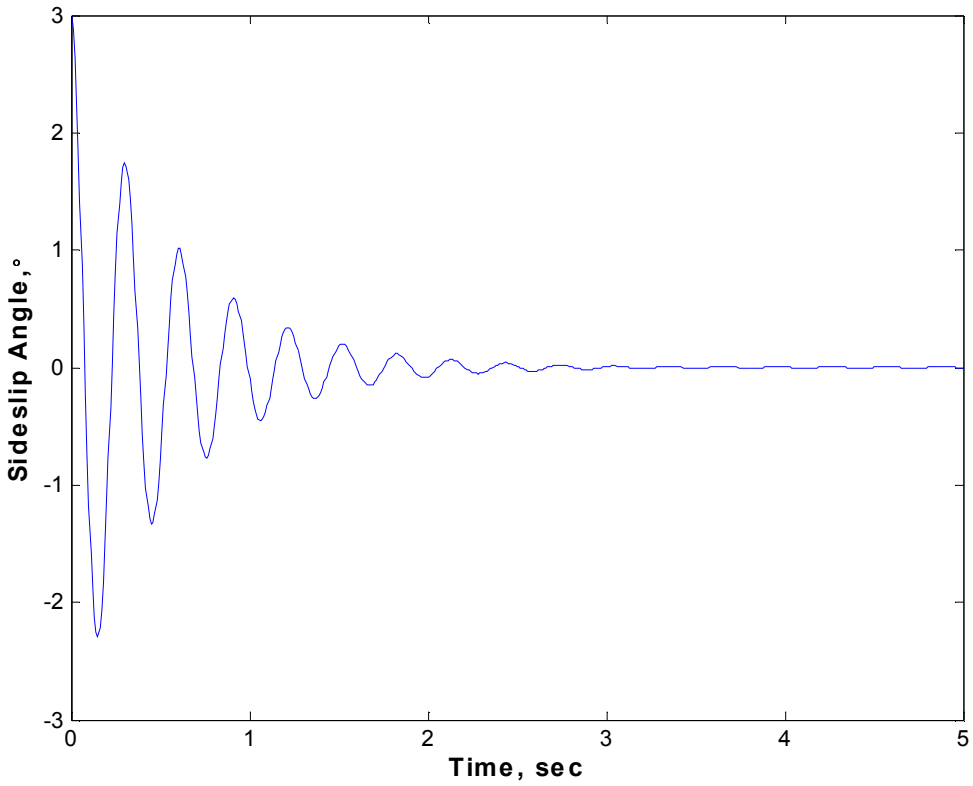

Figure 17. TSA response to initial 3° sideslip (β_{trim} = 0°, M = 1.6, h = 35,000 ft).

Table 10. Six degree-of-freedom dynamic model engine-out trim conditions.

Mach Number	1.6
Altitude (ft)	35,000
Throttle Setting	0.8926
Angle of Attack (°)	0.6244
Elevator Deflection (°)	-1.7220
All-moving Tip Deflection (°)	11
Roll Effector Contribution (C_L)	-0.0115

a)

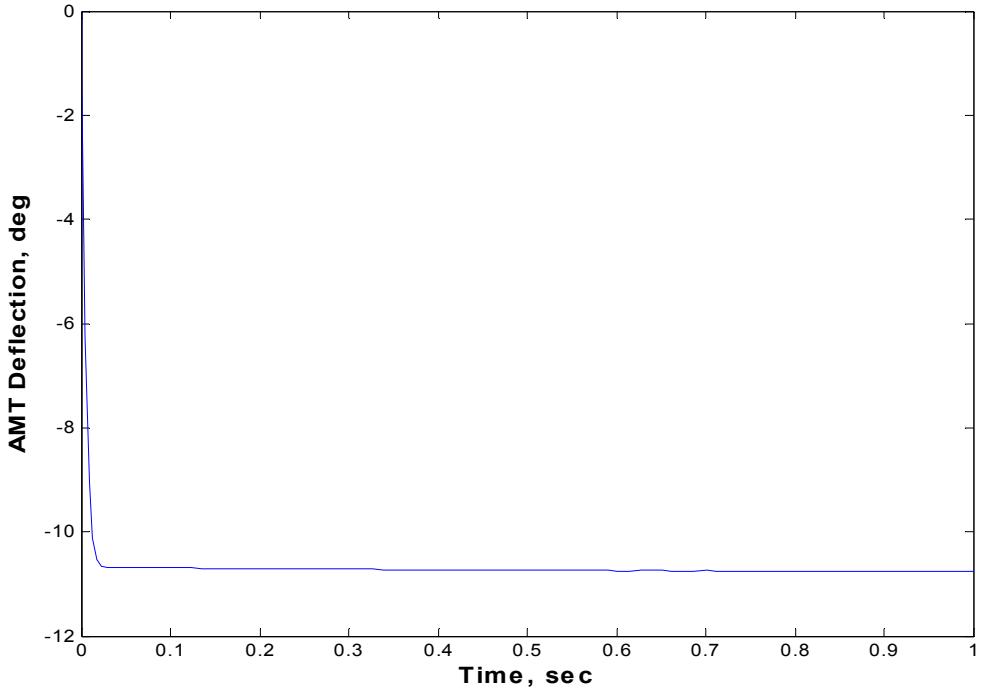

b)

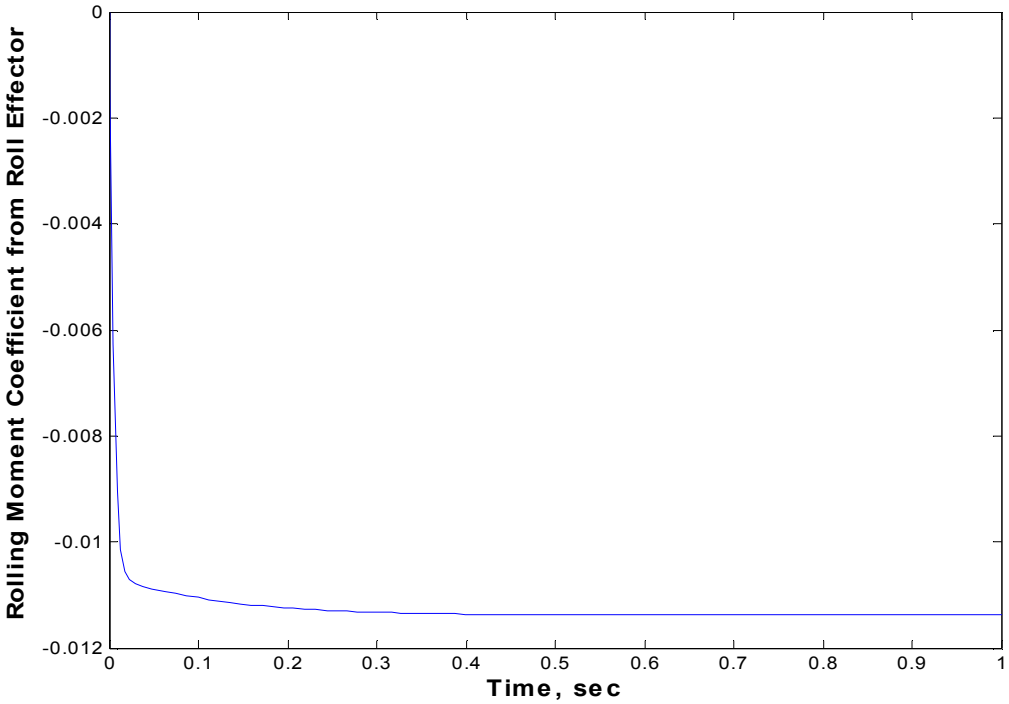

Figure 18. a) All-moving tip and b) roll effector deflections during engine-out simulation (M = 1.6, h = 35,000 ft).

4.3 Actuator Time Constant Study

A study was conducted to determine the effect of the all-moving tip actuator speed on the flying qualities. The goal of this study was to find the slowest actuator that could be used while maintaining Level 1 flying qualities. In the flying qualities examination, roll effector and elevator actuator time constants were held at 0.05 sec while the all-moving tip actuator time constant was varied. The time constants tested ranged from 0.05 sec to 0.318 sec. This range corresponds to actuator bandwidths of 3.181 Hz (τ = 0.05 sec) down to 0.500 Hz (τ = 0.318 sec). Both the spiral and roll subsidence modes met Level 1 flying qualities throughout the test range. However, the Dutch roll mode turned out to be the limiting factor. Dutch roll was tested over a smaller test range to determine the limiting bandwidth more precisely. To meet Level 1 flying qualities, the Dutch roll mode must have a minimum damping ratio of 0.08. The TSA configuration did not meet the minimum Dutch roll damping ratio at AMT actuator bandwidths less than 0.3754 Hz (time constants greater than 0.067 sec). The effects of the AMT actuator time constant on the Dutch roll mode flying qualities are shown in Table 11.

Table 11. All-moving tip actuator effects on Dutch roll flying qualities.

		$\zeta \geq 0.08$	$\omega_n \geq 0.4$	$\zeta\omega_n \geq 0.15$
Time Constant (sec)	**Frequency (Hz)**	**Damping Ratio**	**Natural Frequency (rad/sec)**	$\zeta * \omega_n$
0.05	3.1831	0.0931	17.4245	1.6221
0.05268	3.0212	0.0909	17.4251	1.5839
0.05537	2.8744	0.0888	17.4273	1.5476
0.05805	2.7417	0.0868	17.4304	1.5130
0.06	2.6526	0.0854	17.4334	1.4890
0.06073	2.6207	0.0849	17.4346	1.4802
0.06341	2.5099	0.0831	17.4397	1.4489
0.0661	2.4078	0.0814	17.4455	1.4193
0.067	2.3754	0.0808	17.4476	1.4096
0.06878	2.3140	0.0797	17.4520	1.3911
0.07146	2.2272	0.0781	17.4590	1.3643
0.07415	2.1464	0.0766	17.4665	1.3388
0.07683	2.0715	0.0752	17.4743	1.3146

5. Conclusion

The six degree-of-freedom model was successfully completed for the TSA. The configuration was capable of stable, controlled flight and met all Level 1 flying qualities at the tested flight condition. The TSA used morphing all-moving wingtip control effectors to generate yawing and rolling moment. A trailing edge roll effector was added to suppress excess rolling moment created by the all-moving tips. Alpha/pitch rate feedback was used to improve the longitudinal dynamics. The unstable lateral-directional dynamics were corrected by feeding back yaw rate to the all-moving tips and roll effector. The controller was validated by testing the aircraft response with small perturbations to the trim angle of attack and sideslip angle. The controller was also used to keep the TSA trimmed in case of an engine-out situation. The effects of all-moving tip actuator bandwidth on the lateral-directional dynamics were also examined. Dutch roll damping ratio was determined to be the limiting factor for the all-moving tip actuator speed. Both spiral and roll subsidence modes retained Level 1 flying qualities throughout the test range. The eccentuator concept from the DARPA Smart Wing project is a possible candidate for the morphing all-moving tips actuation system. However, the exact torque and bandwidth specifications of current eccentuators are not known. CFD analysis indicated that over 22,000 ft-lb of torque were required to deflect the all-moving tips to 20° at the test conditions. A future challenge is developing eccentuators capable of meeting the torque and bandwidth requirements of supersonic flight. This analysis of the TSA six degree-of-freedom model and the development of its control system validates the use of all-moving tips as control effectors for supersonic tailless aircraft.

Advances in actuator technology are likely needed before all-moving tips can be used on actual aircraft.

6. Bibliography

[1]Simon, J., Blake, W., and Multhopp, D., "Control Concepts for a Vertical Tailless Fighter," AIAA 93-4000, August 1993.

[2]Bowlus, J., Multhopp, D., and Banda, S. "Challenges and Opportunities in Tailless Aircraft Stability and Control," AIAA-97-3830, 1997.

[3]Gillard, W.J. and Dorsett, K.M., "Directional Control for Tailless Aircraft Using All Moving Wing Tips," AIAA 97-3487, 1997.

[4]Techsburg, Inc., "Morphing Tip Control Effectors for Tailless Supersonic Aircraft," Proposal to BAA AFRL PKV 05-11 Control Effectors for Supersonic Tailless Aircraft, December 2005.

[5]Air Force Research Laboratory, "AFRL Assists Northrop Grumman With Supersonic Tailless Air Vehicle Tests," Retrieved September 28, 2007 from http://www.wpafb.af.mil/news/story.asp?storyID=123055800.

[6]Neel, R., Godfrey, A., and Slack, D. "Turbulence Model Validation in GASP Version 4," AIAA 03-3740, June 2003.

[7]Stevens, B. and Lewis, F., *Aircraft Control and Simulation,* John Wiley & Sons, New York, 1992.

[8]Ashkenas, I. and Klyde, D., "Tailless Aircraft Performance Improvements with Relaxed Static Stability," NASA CR 181806, March 1989.

[9]McRuer, D., Ashkenas, I., and Graham, D., *Aircraft Dynamics and Automatic Control*, Princeton University Press, New Jersey, 1973.

[10]Reichart, R., "Robust Autopilot Design for Aircraft with Multiple Lateral-axes Controls Using H Synthesis," 29th Conference on Decision and Control, Honolulu, Hawaii, December 1990.

[11]Kudva, J.N., "Overview of the DARPA Smart Wing Project," *Journal of Intelligent Material Systems and Structures*, Vol. 15, April 2004.

[12]United States Air Force, *USAF Stability and Control DATCOM*, Flight Control Division Air Force Flight Dynamics Laboratory, Wright-Patterson Air Force Base, Ohio, 1960, rev. 1978.

7. Appendices

7.1 Nomenclature

AMT = all-moving tips, all-moving tip deflection
b = wingspan
$\bar{c}$ = mean aerodynamic chord
$C_1, C_2, \ldots$ = moment of inertia coefficients (see Section 6.2)
C_L = rolling moment coefficient
C_{LP} = roll damping
C_{LR} = roll due to yaw
C_M = pitching moment coefficient
C_{MQ} = pitch damping
$C_{M\alpha}$ = pitching moment change with angle of attack
C_N = yawing moment coefficient
C_{NP} = yaw due to roll
C_{NR} = yaw damping
C_X = axial force coefficient
C_{XQ} = axial force change with pitch rate
C_Y = side force coefficient
C_{YP} = side force due to roll
C_{YR} = side force due to yaw
C_Z = normal force coefficient
C_{ZQ} = normal force change with pitch rate
H_E = angular momentum of engines
I_{xx} = rolling moment of inertia
I_{yy} = pitching moment of inertia
I_{zz} = yawing moment of inertia
I_{xz} = cross-product of inertia
K = control gain
M = Mach number
n = load factor
P = roll rate
Q = pitch rate
$\bar{q}$ = dynamic pressure
R = yaw rate
$REFF$ = roll effector rolling moment coefficient
S = reference area
T = thrust
T_2 = time to double amplitude
$THTL$ = throttle setting

U = axial velocity
u = commanded dynamic state
V = transverse velocity
V_T = true airspeed
W = normal velocity
x = actual dynamic state
x_{cgr} = reference center of gravity
x_{cg} = aircraft center of gravity
z_E = vertical distance from engine to c.g.
α = angle of attack
β = sideslip angle
δe = elevator deflection
τ = time constant
ζ = damping ratio
ω_n = natural frequency

7.2 Moment of Inertia Coefficients

The moment of inertia coefficients are combinations of the aircraft moments of inertia (I_{xx}, I_{yy}, I_{zz}, and I_{xz}) used to simplify the aircraft equations of motion[7].

$$\Gamma = I_{xx} I_{zz} - I_{xz}^{\ 2}$$

$$C_1 = \frac{(I_{yy} - I_{zz}) I_{zz} - I_{xz}^{\ 2}}{\Gamma} \qquad C_2 = \frac{(I_{xx} - I_{yy} + I_{zz}) I_{xz}}{\Gamma} \qquad C_3 = \frac{I_{zz}}{\Gamma}$$

$$C_4 = \frac{I_{xz}}{\Gamma} \qquad C_5 = \frac{I_{zz} - I_{xx}}{I_{yy}} \qquad C_6 = \frac{I_{xz}}{I_{yy}}$$

$$C_7 = \frac{1}{I_{yy}} \qquad C_8 = \frac{I_{xx}(I_{xx} - I_{yy}) + I_{xz}^{\ 2}}{\Gamma} \qquad C_9 = \frac{I_{xx}}{\Gamma}$$

7.3 TSA Dynamic Model (adapted from Ref. 7)

$$C_{XTotal} = C_X(\alpha) + \frac{1}{2}\frac{\bar{c}Q}{V_T}C_{XQ}$$

$$C_{YTotal} = C_Y(\alpha, \beta, x_{AMT}) + \frac{1}{2}\frac{b}{V_T}(C_{YR}R + C_{YP}P)$$

$$C_{ZTotal} = C_Z(\alpha) + \frac{1}{2}\frac{\bar{c}Q}{V_T}C_{ZQ}$$

$$C_{LTotal} = C_L(\alpha, \beta, x_{AMT}) + \frac{1}{2}\frac{b}{V_T}(C_{LR}R + C_{LP}P) + x_{REFF}$$

$$C_{MTotal} = C_M(\alpha, x_{ELEV}) + \frac{1}{2}\frac{\bar{c}Q}{V_T}C_{MQ} + C_{ZTotal}\frac{x_{cgr} - x_{cg}}{\bar{c}}$$

$$C_{NTotal} = C_N(\alpha, \beta, x_{AMT}) + \frac{1}{2}\frac{b}{V_T}(C_{NR}R + C_{NP}P) - C_{YTotal}\frac{x_{cgr} - x_{cg}}{b}$$

$$U = V_T\cos(\alpha)\cos(\beta)$$

$$V = V_T\sin(\beta)$$

$$W = V_T\sin(\alpha)\cos(\beta)$$

$$\dot{U} = RV - QW - g\sin(\theta) + \frac{1}{m}(\bar{q}SC_{XTotal} + T(THTL))$$

$$\dot{V} = PW - RU + g\cos(\theta)\sin(\phi) + \frac{\bar{q}S}{m}C_{YTotal}$$

$$\dot{W} = QU - PV + g\cos(\theta)\cos(\phi) + \frac{\bar{q}S}{m}C_{ZTotal}$$

$$\dot{V}_T = \frac{1}{V_T}(U\dot{U} + V\dot{V} + W\dot{W})$$

$$\dot{\alpha} = \frac{1}{U^2 + W^2}(U\dot{W} - W\dot{U})$$

$$\dot{\beta} = \frac{\cos(\beta)}{U^2 + W^2}(V_T\dot{V} - V\dot{V}_T)$$

$$\dot{\phi} = P + \tan(\theta)(Q\sin(\phi) + R\cos(\phi))$$

$$\dot{\theta} = Q\cos(\phi) - R\sin(\phi)$$

$$\dot{\varphi} = \frac{1}{\cos(\theta)}(Q\sin(\phi) + R\cos(\phi))$$

$$\dot{P} = Q(C_2P + C_1R + C_4H_E) + \bar{q}Sb(C_3C_{LTotal} + C_4C_{NTotal})$$

$$\dot{Q} = R(C_5P - C_7H_E) + C_6(R^2 - P^2) + \bar{q}S\bar{c}C_7C_{MTotal}$$

$$\dot{R} = Q(C_8P - C_2R + C_9H_E) + \bar{q}Sb(C_4C_{LTotal} + C_9C_{NTotal})$$

$$\dot{h} = U\sin(\theta) - V\sin(\phi)\cos(\theta) - W\cos(\phi)\cos(\theta)$$

$$u_{ELEV} = -K_\alpha(\alpha - \alpha_{trim}) - K_q(Q - Q_{trim}) + ELEV_{trim}$$

$$u_{AMT} = K_{AMT}(R - R_{trim}) + AMT_{trim}$$

$$u_{REFF} = K_{REFF}(R - R_{trim}) + REFF_{trim}$$

$$\dot{x}_{ELEV} = \frac{u_{ELEV} - x_{ELEV}}{\tau_{ELEV}}$$

$$\dot{x}_{AMT} = \frac{u_{AMT} - x_{AMT}}{\tau_{AMT}}$$

$$\dot{x}_{REFF} = \frac{u_{REFF} - x_{REFF}}{\tau_{REFF}}$$

Vita

Brady Alexander White was born in Greenville, South Carolina on July 4, 1984 to Cyndi Floyd White and Donald Kent White. He attended Wren High School in Piedmont, South Carolina and graduated in May 2002. After completing high school, he entered the Virginia Tech College of Engineering. Brady graduated summa cum laude in May 2006 with a Bachelor of Science degree in aerospace engineering. Upon completing his undergraduate work, he entered graduate school at Virginia Tech pursuing a Master of Science degree in aerospace engineering.